Observed Patterns of Heat Wave Intensities with Respect to Time and Global Surface Temperature

Gioia Di Credico and Francesco Pauli

Abstract In studying climate change effects, it is crucial to analyze not only the average behavior of weather but also extreme phenomena like heat waves. This paper examines the relationship between heat wave intensity and either time and global surface temperature. We present preliminary findings based on a limited number of locations and a single measure of heat wave. We note that trends in extreme phenomena differ from average trends and vary across different locations. The study emphasizes the importance of understanding and monitoring heat wave intensities in relation to time and global surface temperature to evaluate the impacts of these extreme weather events properly.

Keywords Bayesian inference · Free-knots splines · Knot location · Truncated linear basis

1 Introduction

In studying the impact of climate change, it is relevant to analyze not only the mean behavior of weather, e.g., the average temperature or precipitation, but also the extreme behavior, such as the occurrence of heat waves (HWs). The relevance of specifically investigating extreme phenomena is twofold. On the one hand, extreme phenomena directly affect the human population; HWs have been projected to be Europe's main source of weather-related disasters in terms of exposed population and mortality [2]. On the other hand, trends in extreme phenomena may differ from the trend in the corresponding averages and from one location to the other in various ways. According to the literature, depending on the location, HWs may or may not increase in duration and intensity, and, in a few locations, they may also decrease. Furthermore, the growth, when present, may accelerate in the last decades, since the 80s or 90s typically [5]. In the following, we analyze observed HWs in selected

G. Di Credico (✉) · F. Pauli
DEAMS, University of Trieste, Trieste, Italy
e-mail: gioia.dicredico@deams.units.it

locations in the period from 1950 to 2021 with a flexible non-linear model to detect the rate of increase of the phenomenon and the shape of the trend, in particular, its potential non-linearity.

Also, it has been noted that at least in some regions of Europe, the hottest day temperature is increasing more rapidly than the mean daily temperature [4]. HWs are a more complex phenomenon than the maximum daily temperature, so they do not necessarily follow the same pattern. This is investigated in this work by modeling the relationship between HWs and global surface temperature (GST) in selected locations.

In studying HWs, a significant complication arises since HWs are a complex phenomenon: broadly speaking, an HW is a prolonged period of time during which the temperature is above a high threshold. Thus, its duration and intensity can describe an HW, and its measures depend on a conventional choice of a threshold above which the temperature is considered high. In the literature, multiple yearly summaries of HWs have been considered: the count, the mean/maximum/cumulative duration, and the mean/maximum/cumulative intensity (degrees above a given threshold, either constant or relative). A comparison of the results across different choices of the measure is out of scope for the present work, so we focus on the yearly maximum intensity (for each HW, the maximum intensity is the difference between the temperature of the hottest day and the threshold; these excesses are then averaged across all the HWs of the year). This choice is mainly driven by convenience, as the distribution of the variable can be reasonably approximated using a Gaussian model.

We compute this measure for summer HWs (i.e., HWs occurring between May and September of each year) based on data from the Berkeley Earth Surface Temperature dataset [6] for four locations in the European region, which are in the following identified by the name of the Country they fall in.

2 Methods

In a Gaussian regression model, several alternatives exist to evaluate and eventually relax a predictor's linear effect on the response variable. Spline functions of order two are well suited to represent piecewise linear relationships avoiding the restrictive predictor categorization while preserving the ease of coefficients interpretation. A spline function is constructed connecting piecewise functions at knot locations. In the following, we consider a spline of order two; therefore, the piecewise functions are linear, and each knot identifies a slope change with respect to the previous regime, also implying a discontinuity in the first derivative at the knot locations. The truncated linear basis (TLB) representation identifies a change in the effect with each knot and, with the corresponding coefficient, the difference in the slope after the knot. This representation comes with some drawbacks but is particularly attractive when the analysis focuses on the interpretation of the model. To prevent problems related to the correlation that can arise between the components of the truncated basis, it is advisable to limit its use when the expected number of changes is low. When the

number of knots is fixed, we can treat knot locations as parameters and estimate them along with other regression and spline coefficients.

Under the Bayesian framework, we define a linear regression model with TLB spline and K free-knots as follows:

$$y_i|\beta_0, \beta_1, \boldsymbol{\gamma}, \boldsymbol{\xi}, \sigma^2 \overset{\text{ind.}}{\sim} N\left(\beta_0 + x_i\beta_1 + \sum_{k=1}^{K}(x_i - \xi_k)_+\gamma_k, \sigma^2\right), \tag{1}$$

for $i = 1, \ldots, n$, and $k = 1, \ldots, K$, where $\mathbf{y}$ is the response variable, i.e., in our study, the maximum yearly temperature of the HWs, $\mathbf{x}$ is a continuous predictor, the years from 1950 to 2021 or the GST in the two models we consider, while the function $(x_i - \xi_k)_+ = (x - \xi_k)\mathrm{I}(x \geq \xi_k)$ represents the TLB elements for each knot location ξ_k. The parameters β_0 and β_1 are the intercept and the predictor coefficient, $\boldsymbol{\gamma}$ is the vector of the spline coefficients linked with the TLB, and σ^2 is error variance.

The prior distributions for the parameters β_0, β_1, $\boldsymbol{\gamma}$, and σ^2 comply the weakly informative prior setting suggested by [3], that is

$$\beta_0 \sim N\left(\bar{y}, 10s_y\right), \quad \beta_1 \sim N\left(0, 2.5s_y/s_x\right), \tag{2}$$

$$\gamma_k|\xi_k \sim N\left(0, 2.5s_y/s_{\xi[k]}\right), \quad \sigma \sim \exp\left(1/s_y\right), \tag{3}$$

where s_y and s_x are the standard deviations of the response and the predictor, respectively, and $s_{\xi[k]}$ is the one evaluated on the kth TLB term. The autoscale characteristic of these priors automatically accounts for the different scales of the TLB terms. Lastly, uninformative prior distributions subject to identifiability constraints are set on the knot locations $\boldsymbol{\xi}$

$$\xi_k \sim Unif(min(\boldsymbol{x}), max(\boldsymbol{x})), \quad \text{subject to } \xi_k < \xi_{k+1}, \tag{4}$$

for $k = 1, \ldots, K-1$. For a fixed number of knots, this model specification is used to obtain posterior estimates of the location of the knots along with the other model parameters.

The selection of the number of knots relies on comparing models with different numbers of changing points through the approximate leave-one-out cross-validation (LOO) information criterion, opting for the model with the lowest LOO value [7].

3 Applications

We examine how the yearly HW maximum intensity changes over time and in relation to the GST in four different European locations. In the following, we identify them by the Country in which they are: Finland, Netherlands, Spain, and Turkey. More

in detail, the geographical coordinates of the four grid cells are: Finland [26°–27° E, 67°–68° N], Netherlands [6°–7° E, 52°–53° N], Spain [0°–1° W, 38°–39° N], Turkey [42°–43° E, 40°–41° N]. It is worth noting that the results should be referred to the single cells, which are not representative of the surrounding area or the entire State. The analyzed period covers 72 years, starting from 1950 up to 2021, with few missing values on each series. The sample size in each location is 66 for Finland, 68 for Netherlands and Spain, and 61 for Turkey.

We simulate models with zero, one, and two free-knots using the NUTS algorithm [1]. Inference is based on the 8000 sampling draws obtained from 4 chains, each with a warm-up step of 2000 iterations. First, posterior diagnostic checks are performed to exclude possible sampling issues, then the final models are selected by comparing their LOO information criterion values, choosing the lowest one.

3.1 Heat Wave Maximum Intensity Over Time

Figure 1 clearly shows that the yearly HW maximum intensity is characterized by different patterns over time in the four locations: an acceleration in the increase of the phenomenon is detected in Turkey and the Netherlands but not in Spain and Finland. This intuition is supported by the LOO information criterion values that suggest selecting the one-knot spline models for Netherlands and Turkey data and the linear model for Finland and Spain cases (Table 1). The behavior is also confirmed by the curves estimated with generalized additive models (GAMs) that mostly overlap the piecewise linear spline curves (Fig. 1). Note that, due to the limited sample size, we increased the value of the parameter `gamma` to prevent overfitting in the GAM as suggested by [8]. In all four models, the β_1 coefficients estimates are not different from 0. Therefore we do not report them along with the other coefficients posterior estimates (Table 2). This highlights a constant behavior on average of the HW maximum intensity over the entire period for Finland and Spain and constant up to the knot for the Netherlands and Turkey. The estimates of the coefficients linked with the TLB basis terms are concentrated on positive values, as their 95% quantile-based credible intervals. The estimates interpretation is straightforward: after the knot, the expected increases in the HW maximum intensities every ten years are about 1 degrees in the Turkey cell and 0.5 in the Netherlands one. The posterior medians of the knot locations are equal to 1979 for the Netherlands and

Table 1 HW maximum intensity over time: LOO information criterion of the fitted models with a different number of knots K. Bold numbers indicate the selected models

K	Finland	Netherlands	Spain	Turkey
0	**242.42**	213.42	**182.25**	172.54
1	243.90	**208.63**	183.17	**164.98**
2	244.93	209.20	183.38	165.87

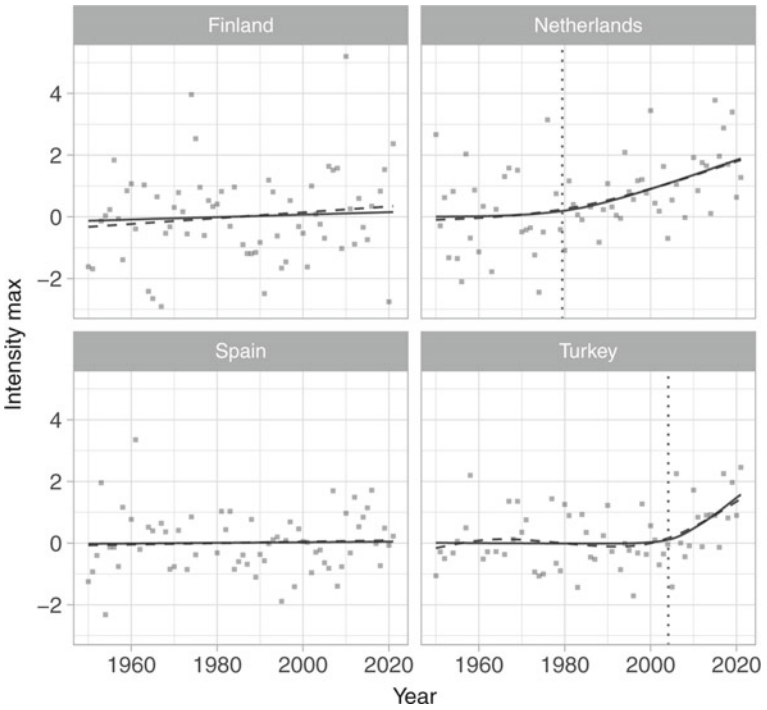

Fig. 1 HW maximum intensity over time for the four locations in analysis (*grey dots*). The plot shows the median posterior estimates obtained from the models with linear trend, for Finland and Spain, and free-knots spline, for the Netherlands and Turkey, (*solid line*) along with estimated knot locations (*vertical dotted line*). The curve estimated with a GAM is represented with a *dashed line*. The quantities have been centered with respect to the specific location mean

2004 for Turkey. However, the posterior distribution of these knot locations looks more asymmetric and more spread for the Netherlands than for Turkey (Fig. 2).

It is interesting to note that the time trend accelerates in some areas, as expected, but not everywhere, and the time in which the slope changes is also estimated at different years. This non-uniformity of the magnitudes and shape of the increase is also not new [5]. However, further analysis is needed to assess whether this heterogeneity is structural. Further model diagnostic plots are available in the Appendix (Figs. 4–7).

3.2 Heat Wave Maximum Intensity and Global Surface Temperature

When the HW maximum intensity is related to the GST, the models recommended by the LOO information criterion are linear in all locations (Table 3). The models

Table 2 HW maximum intensity over time: posterior estimates of the model coefficients, namely, posterior mean and standard deviation, and posterior quantiles of order 0.025 ($Q_{2.5\%}$), 0.5 ($Q_{50\%}$), and 0.975 ($Q_{75\%}$)

Country	Parameter	Posterior mean	sd	$Q_{2.5\%}$	$Q_{50\%}$	$Q_{97.5\%}$
Finland	β_0	0.94	11.27	−20.86	0.84	23.76
Netherlands	β_0	8.28	13.04	−16.73	8.02	34.71
	γ_1	0.05	0.03	0.02	0.05	0.12
Spain	β_0	2.94	7.36	−11.27	2.71	17.90
Turkey	β_0	6.73	8.74	−10.18	6.71	23.98
	γ_1	0.13	0.22	0.02	0.10	0.36

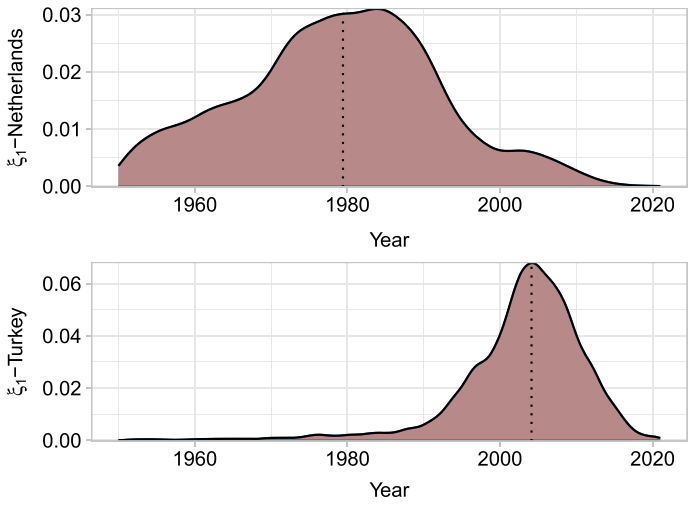

Fig. 2 HW maximum intensity over time: kernel density estimates of the posterior distributions and posterior median estimates for the two knot locations identified for Netherlands and Turkey cells at 1979 and 2004, respectively (*vertical dotted lines*)

reflect what observed in the previous analysis: the strongest increasing trends are found in Netherlands and Turkey (Fig. 3). Also in this case, the GAM estimates overlaps with the curves estimated with the piecewise linear spline model. Further model diagnostic plots are available in the Appendix (Figs. 8–11).

The fact that the coefficient of GST is near to two in the Netherlands, approximately equal to one in Turkey, and lower in Finland and Spain is broadly in line with the results of [4] who compared the rate of increase of the maximum temperature and the mean temperature, highlighting that in the North-West region of Europe the former increases twice as rapidly as the latter (Table 4).

Table 3 HW maximum intensity and GST: LOO information criterion of the fitted models with a different number of knots K. Bold numbers indicate the selected models

K	Finland	Netherlands	Spain	Turkey
0	**244.65**	**208.23**	**182.87**	**169.11**
1	246.52	210.07	184.175	169.53
2	247.43	210.46	184.61	169.04

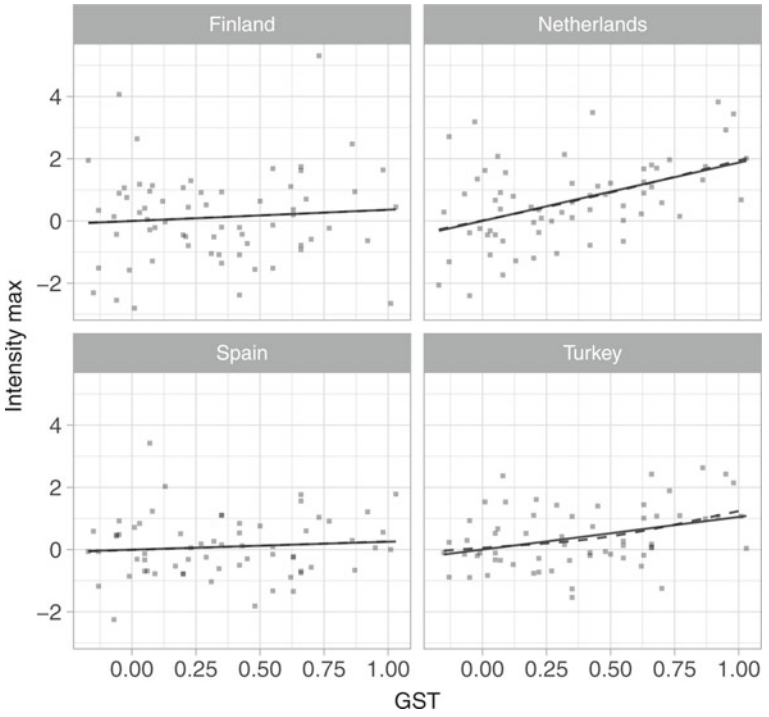

Fig. 3 HW maximum intensity and GST for the four locations in analysis (*grey dots*). The plot shows the median posterior estimates obtained from the models all with linear trend (*solid line*). The curve estimated with a generalized additive model is represented with a *dashed line*. The quantities have been centered with respect to the specific location mean

4 Conclusions

We have analyzed HWs intensity patterns over the last seven decades employing a flexible regression model particularly suitable to detect the position and the magnitude of possible transitions in the rate of change of the phenomenon of interest. This feature is particularly relevant for HWs from a substantive point of view.

Table 4 HW maximum intensity and GST: posterior estimates of the model coefficients, namely, posterior mean and standard deviation, and posterior quantiles of order 0.025 ($Q_{2.5\%}$), 0.5 ($Q_{50\%}$), and 0.975 ($Q_{75\%}$)

Country	Parameter	Posterior mean	sd	$Q_{2.5\%}$	$Q_{50\%}$	$Q_{97.5\%}$
Finland	β_0	8.62	0.27	8.09	8.62	9.16
	β_1	0.36	0.58	−0.77	0.37	1.49
Netherlands	β_0	8.47	0.21	8.06	8.47	8.90
	β_1	1.87	0.46	0.98	1.87	2.79
Spain	β_0	4.68	0.18	4.33	4.68	5.03
	β_1	0.26	0.37	−0.47	0.26	0.98
Turkey	β_0	5.00	0.18	4.63	5.00	5.35
	β_1	1.05	0.37	0.33	1.05	1.79

The results of the analysis are broadly in line with the existing literature in showing: (1) non-uniform growth rates across different locations; (2) an accelerated growth in the last decades in some locations; (3) a growth more rapid than that of the GST in the North-West of Europe. The modeling strategy we employed also allows inference for the starting year of accelerated growth, which is estimated in 1979 for Turkey and later (2004) for the Netherlands, suggesting geographical non-homogeneity also concerning this phenomenon feature.

These results are preliminary and suffer many limitations, which will be dealt with in future extensions. We examine a few locations and do not attempt to model the spatial aspect. Furthermore, we consider only one measure of HW, while other dimensions of the phenomenon may be examined, such as the HW duration, frequency, or cumulative intensity. Lastly, we relate HWs and GST, but a more relevant measure might be the yearly average maximum daily temperature specific to the cell.

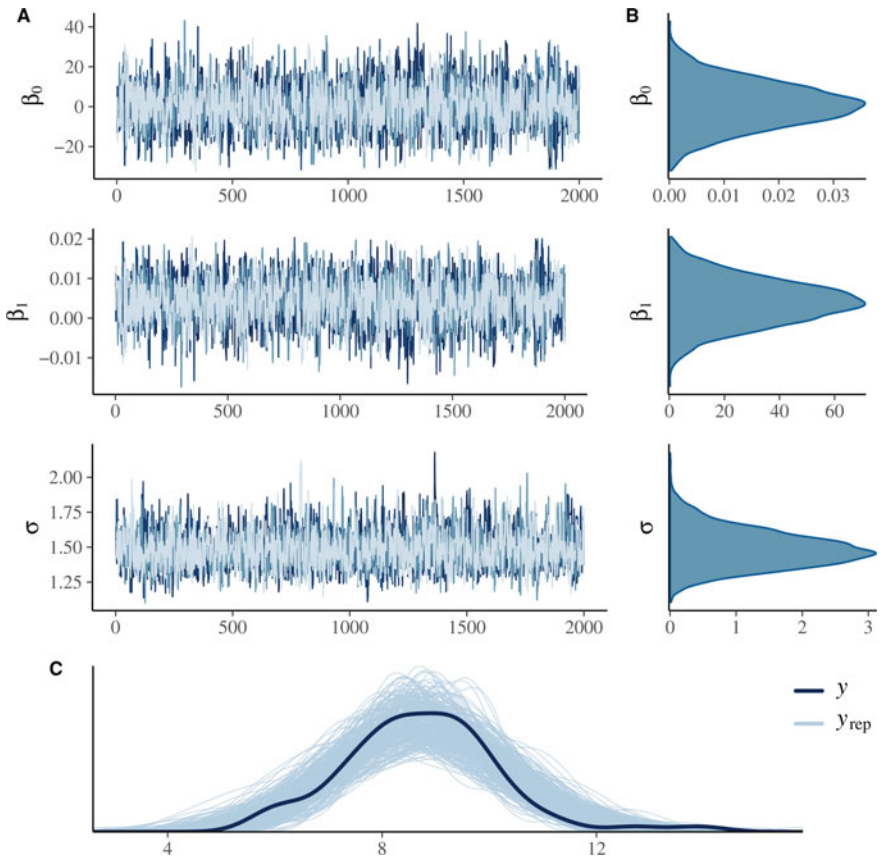

Fig. 4 Yearly maximum intensity over time for Finland. Selected diagnostic checks: trace plots (**A**) and marginal posterior densities (**B**) for the main model parameters and posterior predictive checks compared with the observed data (**C**)

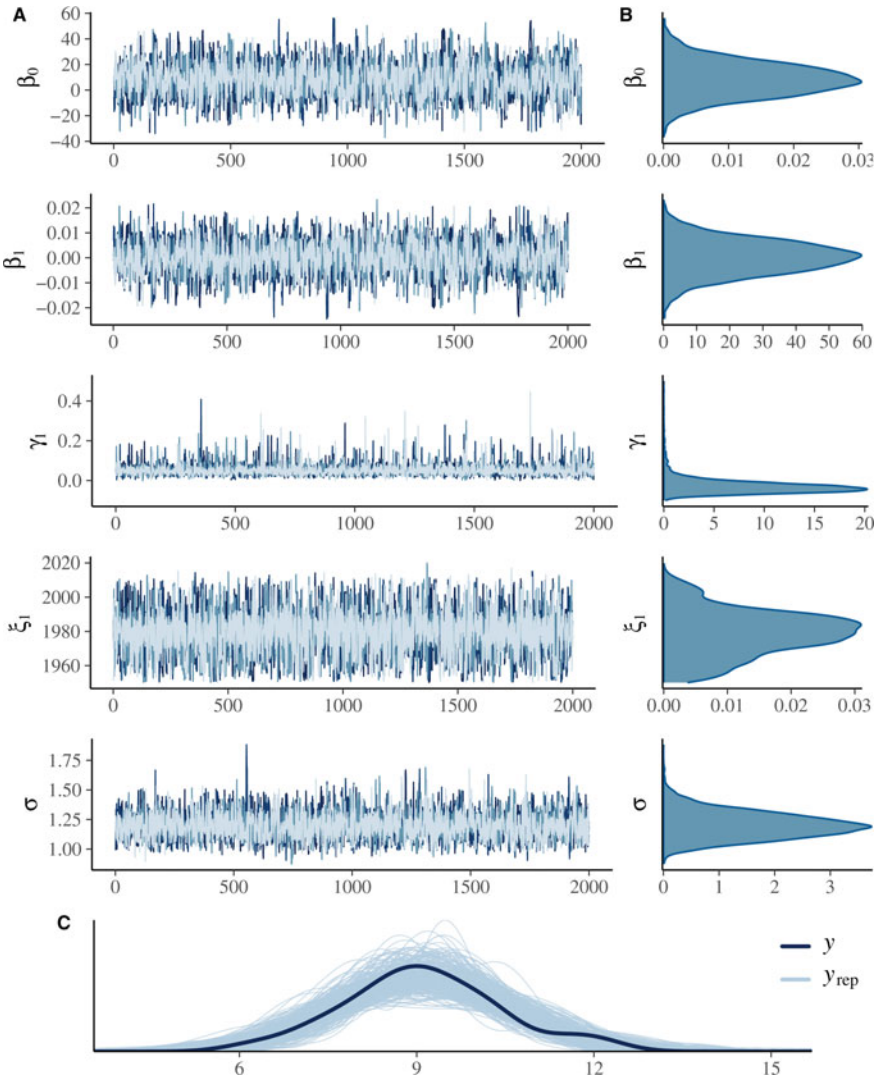

Fig. 5 Yearly maximum intensity over time for Netherlands. Selected diagnostic checks: trace plots (**A**) and marginal posterior densities (**B**) for the main model parameters and posterior predictive checks compared with the observed data (**C**)

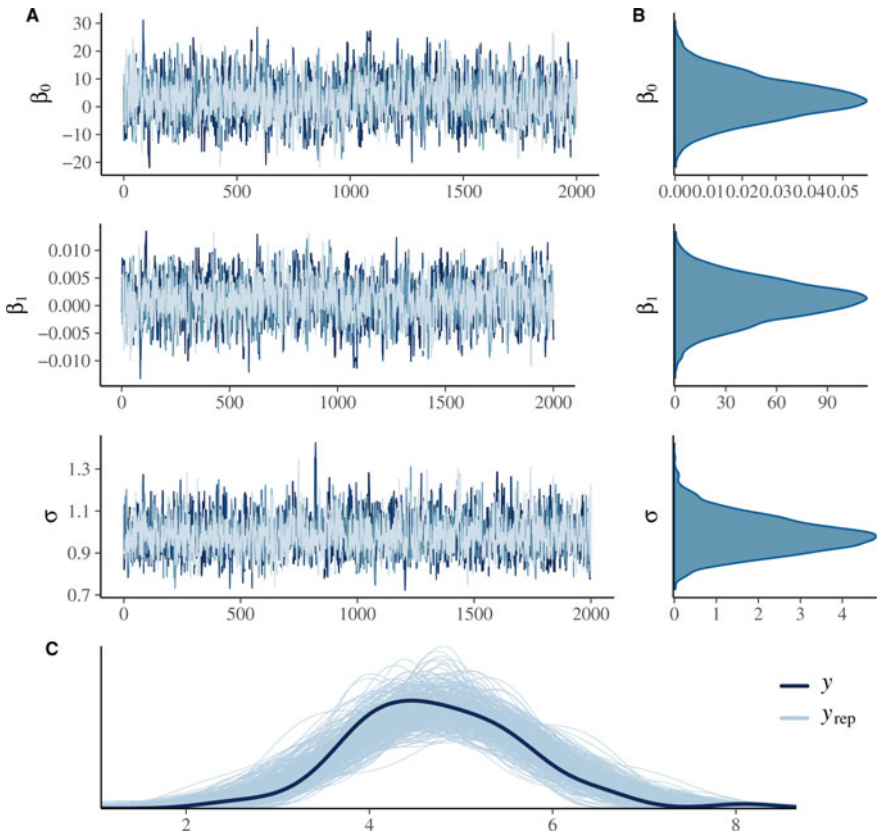

Fig. 6 Yearly maximum intensity over time for Spain. Selected diagnostic checks: trace plots (**A**) and marginal posterior densities (**B**) for the main model parameters and posterior predictive checks compared with the observed data (**C**)

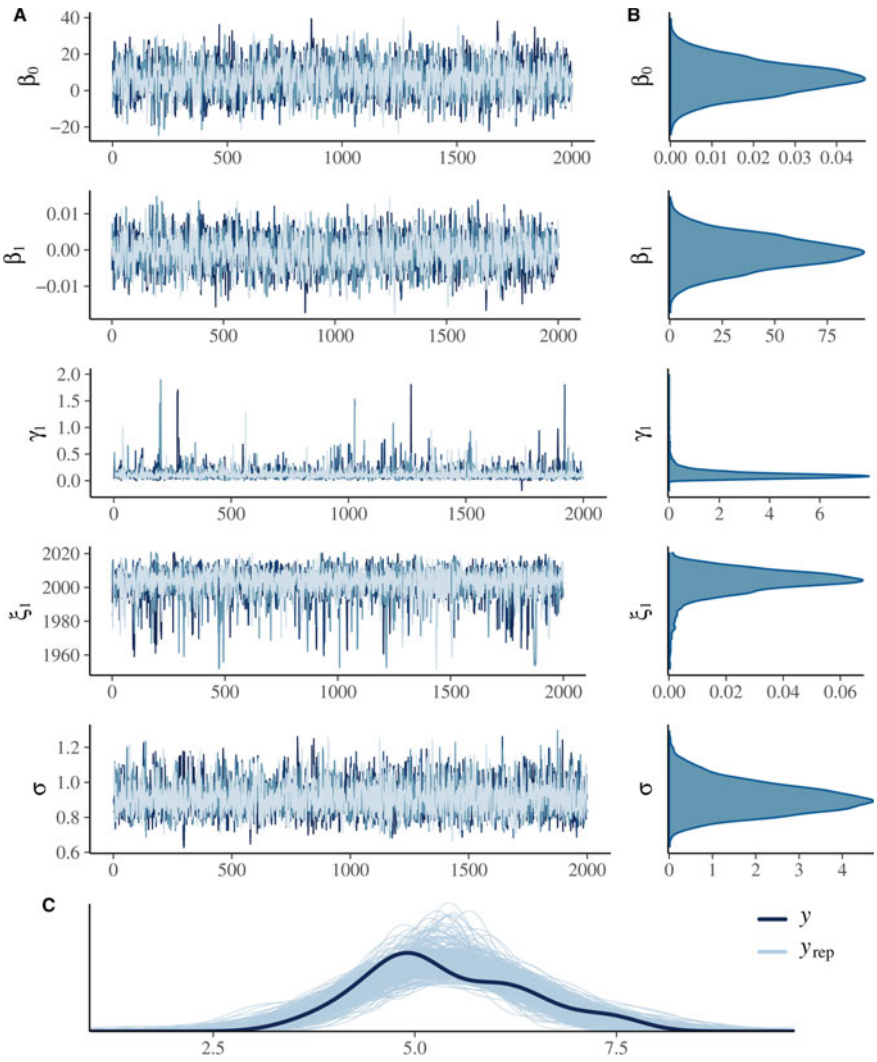

Fig. 7 Yearly maximum intensity over time for Turkey. Selected diagnostic checks: trace plots (**A**) and marginal posterior densities (**B**) for the main model parameters and posterior predictive checks compared with the observed data (**C**)

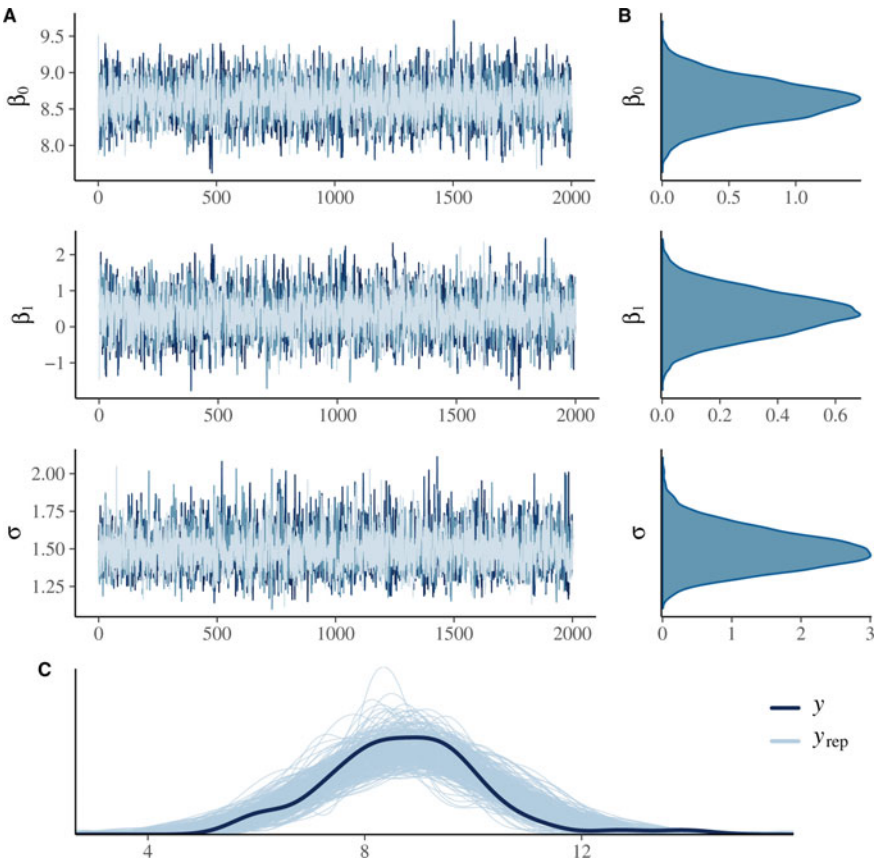

Fig. 8 Yearly maximum intensity versus GST for Finland. Selected diagnostic checks: trace plots (**A**) and marginal posterior densities (**B**) for the main model parameters and posterior predictive checks compared with the observed data (**C**)

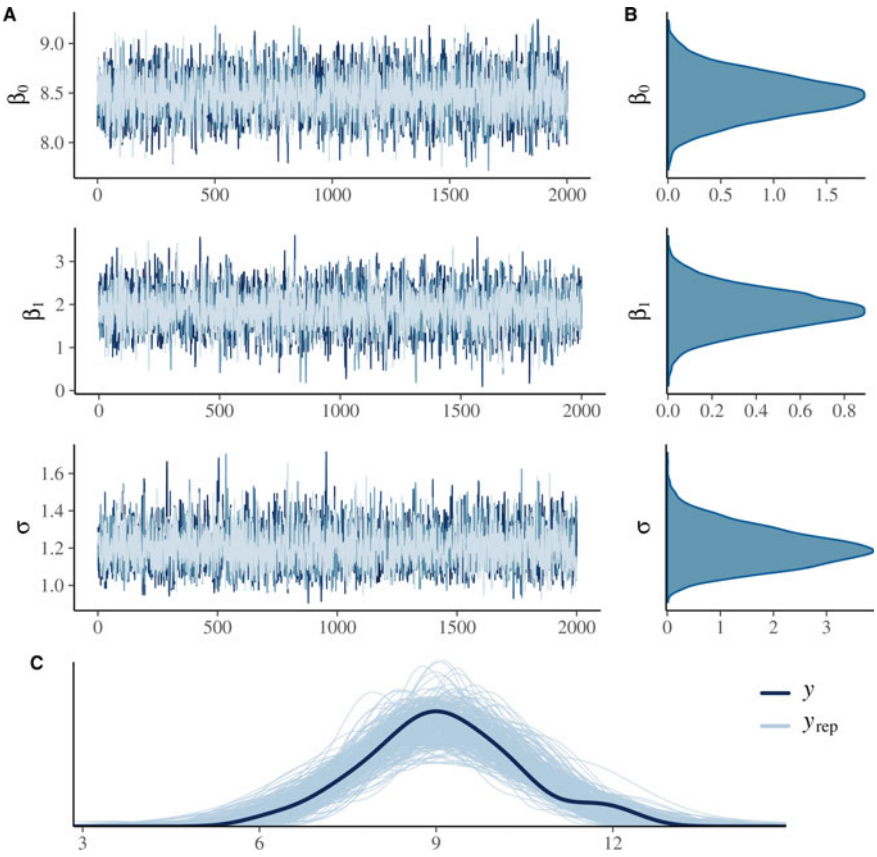

Fig. 9 Yearly maximum intensity versus GST for Netherlands. Selected diagnostic checks: trace plots (**A**) and marginal posterior densities (**B**) for the main model parameters and posterior predictive checks compared with the observed data (**C**)

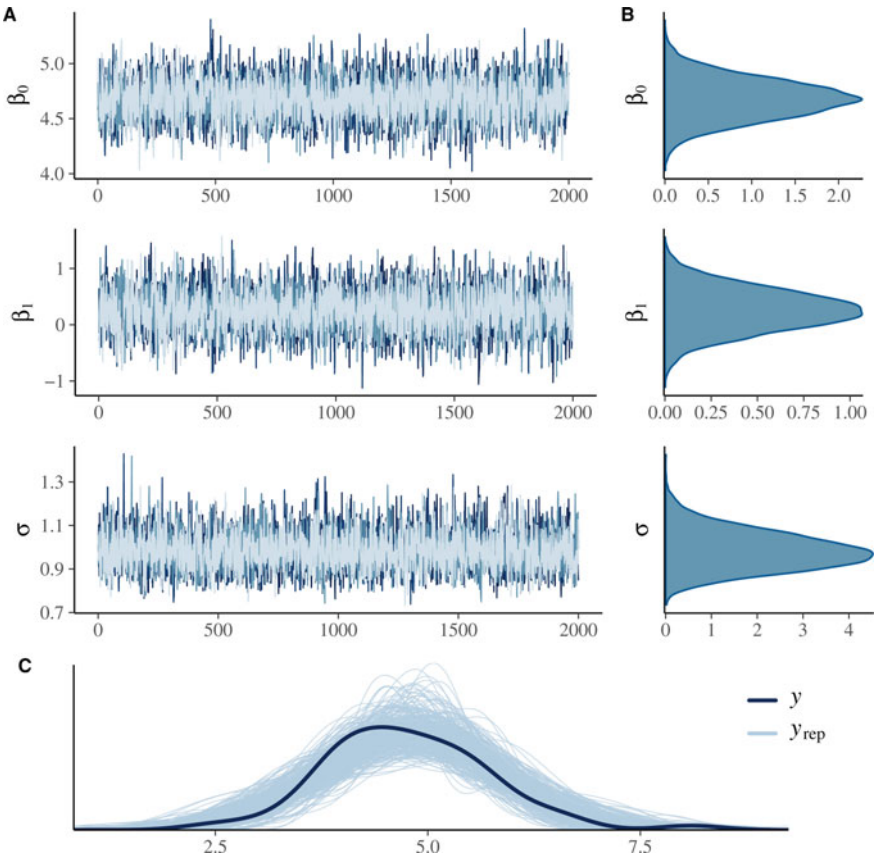

Fig. 10 Yearly maximum intensity versus GST for Spain. Selected diagnostic checks: trace plots (**A**) and marginal posterior densities (**B**) for the main model parameters and posterior predictive checks compared with the observed data (**C**)

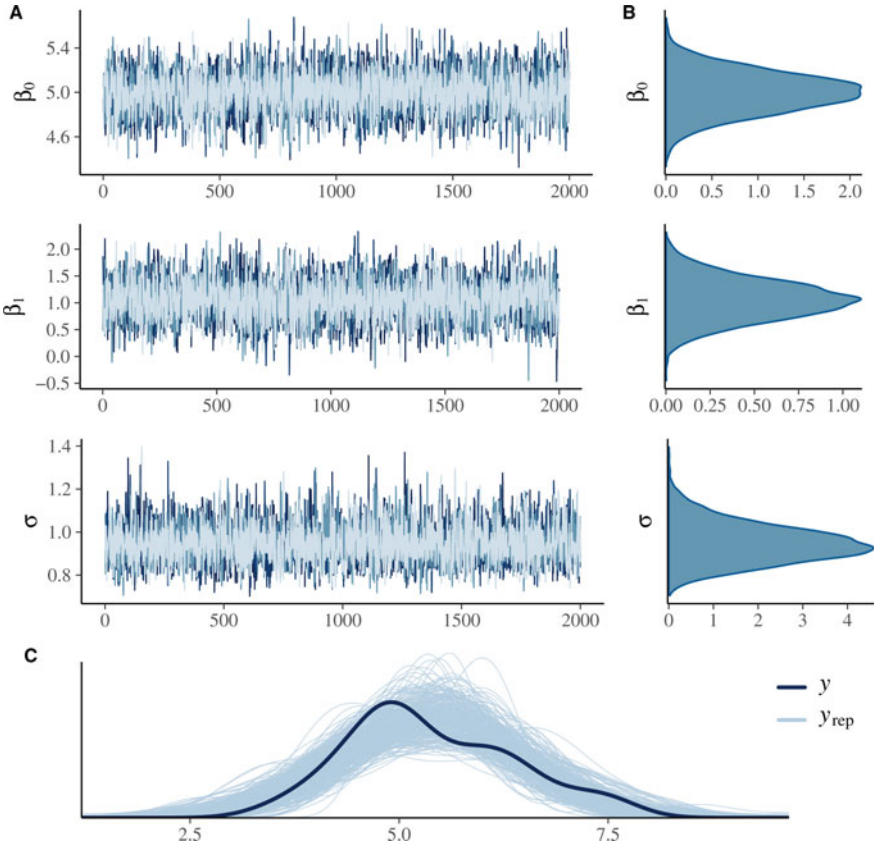

Fig. 11 Yearly maximum intensity versus GST for Turkey. Selected diagnostic checks: trace plots (**A**) and marginal posterior densities (**B**) for the main model parameters and posterior predictive checks compared with the observed data (**C**)

References

1. Carpenter, B., Gelman, A., Hoffman, M.D., Lee, D., Goodrich, B., Betancourt, M., Brubaker, M., Guo, J., Li, P., Riddell, A.: Stan: a probabilistic programming language. J. Stat. Softw. **76**, 1–32 (2017). https://doi.org/10.18637/jss.v076.i01
2. Forzieri, G., Cescatti, A., Silva, F.B., Feyen, L.: Increasing risk over time of weather-related hazards to the European population: a data-driven prognostic study. Lancet Planet. Health **1**, e200–e208 (2017). https://doi.org/10.1016/S2542-5196(17)30082-7
3. Gelman, A., Hill, J., Vehtari, A.: Regression and Other Stories. Cambridge University Press (2020). https://doi.org/10.1017/9781139161879
4. Patterson, M.: North-West Europe hottest days are warming twice as fast as mean summer days. Geophys. Res. Lett. **50** (2023). https://doi.org/10.1029/2023GL102757
5. Perkins-Kirkpatrick, S.E., Lewis, S.C.: Increasing trends in regional heatwaves. Nat. Commun. **11**, 3357 (2020). https://doi.org/10.1038/s41467-020-16970-7

6. Rohde, R., Muller, R., Jacobsen, R., Perlmutter, S., Rosenfeld, A., Wurtele, J., Curry, J., Wickham, C., Mosher, S.: Berkeley earth temperature averaging process. Geoinformatics Geostati. Overv. **1**, 20–100 (2013). https://doi.org/10.4172/gigs.1000103
7. Vehtari, A., Gelman, A., Gabry, J.: Practical Bayesian model evaluation using leave-one-out cross-validation and WAIC. Stat. Comput. **27**, 1413–1432 (2017). https://doi.org/10.1007/s1122201696964
8. Wood, S.N.: Generalized Additive Models: An Introduction with R. CRC Press (2017)